Adaptative Resonant Tank of Bidirectional CLLC Resonant Converters for Electric Vehicle Charging Applications

Borja Prietoº*, Ander Ávilaº, David Garrido*, Iosu Aizpuru*, Alejandro Rujasº
ºIkerlan Technology Research Centre Basque Research Technology Alliance (BRTA) / Arrasate-Mondragón, Spain
*Electronics and Computing Department Mondragon Unibertsitatea / Hernani, Spain
Tel.: +34 / 943712400.
E-Mail: bprieto@ikerlan.es
URL: https://www.ikerlan.es/ ; https://www.mondragon.edu/en/home

Acknowledgment

The ALL2GaN Project (Grant Agreement No 101111890) is supported by the Chips Joint Undertaking and its members including the top-up funding by Austria, Belgium, Czech Republic, Denmark, Germany, Greece, Netherlands, Norway, Slovakia, Spain, Sweden and Switzerland. Funded by the European Union. Views and opinions expressed are however those of the author(s) only and do not necessarily reflect those of the European Union, Chips JU or the national granting authorities. Neither the European Union nor the granting authorities can be held responsible for them.

This paper has been supported by the government of the Basque Country through the research grant BIKAINTEK 014-B2/2024 (Análisis y optimización de convertidores resonantes con carga variable para aplicaciones con un amplio rango de tensión).

***Index Terms*—DC-DC, Resonant converter, CLLC resonant converter, Reconfigurable resonant network.**

***Abstract*—This paper focuses on optimizing the design of CLLC converters for asymmetric bidirectional operation, a critical requirement in electric vehicle (EV) charging systems. Previous research has shown that CLLC converters are effective due to their soft-switching characteristic, achieving high performance in terms of efficiency and power density. However, challenges remain in optimizing their operation for bidirectional power flow, particularly for wide voltage and load applications such as vehicle-to-grid (V2G). To address this, we evaluate a novel approach that adds a parallel inductor to the primary side of the resonant tank in reverse operation to improve the gain characteristics and efficiency. The research uses theoretical analysis and simulations. The results show a resonant converter capable of meeting the requirements of a wide voltage and load range application without compromising the performance of the main operating mode, all while keeping the magnetizing/leakage inductance relation within the design criteria for integrated transformers.**

I. Introduction

The rapid adoption of electric vehicles (EVs) has increased the demand for efficient, high-power density chargers that can operate across wide load and voltage ranges. These chargers are also required to have galvanic isolation, which prevents leakage currents that may be a risk for the user in order to comply with safety standards and regulations. Additionally, the need for bidirectionality keeps increasing due to the fact that EVs connected to the grid offer a vast battery network that can be used to provide the grid with active or reactive power in high-demand, voltage and frequency regulation, or current harmonic reduction applications [1]–[3].

In this area, resonant converters have emerged as a promising solution due to their inherent soft-switching characteristics over wide voltage and load ranges, reduced harmonic content, high efficiency, providing nearly no energy loss in both directions, especially at the nominal working point, and compact size [4]–[6]. In applications requiring bidirectionality, such as the one depicted in Fig. 1, CLLC converters are strong competitors, offering the advantages of LLC resonant converters in both forward and reverse power flow directions [4], [7], [8].

Moreover, compared to the dual active bridge (DAB) converter, its main competitor in this field, the CLLC resonant converter, offers better nominal power performance with less high-order harmonic ripple content, a

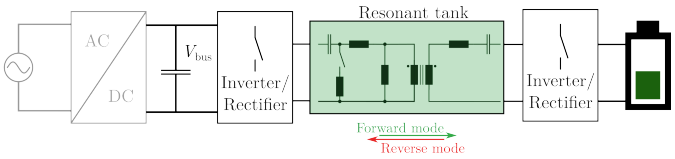

Fig. 1. Proposed bidirectional battery charging system, with a reconfigurable CLLC resonant tank.

result of the nearly sinusoidal waveforms in the tank. This will also have a positive impact on the output filter requirements of the converter, resulting in a higher power density. On top of that, DAB tends to lose zero voltage switching (ZVS) in partial load conditions, so a wider ZVS range is usually obtained in CLLC converters which results in better overall efficiency considering the whole power range of the system [5], [9]–[11].

However, the performance of CLLC converters is highly dependent on key parameters such as the switching frequency and the selection of the resonant tank components. The gain of the converter can be enhanced by increasing the range of the switching frequency and/or decreasing the value of the resonant tank inductances. Nevertheless, the efficiency of resonant converters decreases when operating over a wide frequency range, especially as the difference between the switching frequency and the resonant frequency increases. Not only that, but a wide switching frequency range can make component optimization challenging. This can lead to the loss of the power density benefits of a CLLC converter if a very low switching frequency is needed. Additionally, it is limited on the higher side by the current switching-device technology [12]. Furthermore, a reduced value of the inductances in the resonant tank implies higher currents through the converter. This critically affects the system's performance and design by increasing power losses and complicating the selection of switching components and the design of passive components, which must handle higher currents.

However, one of the most critical factors in a bidirectional application is that the gain needs of the resonant tank may not be the same for both power directions [13]. This makes the system's design suboptimal, as the same configuration needs to suit the forward and reverse mode requirements. Consequently, the design for one of the directions will be restrained by the other, resulting in lower resonant tank inductances compared to an optimum unidirectional design, and the mentioned efficiency consequences [14].

These factors become crucial when the wide input voltage or load variations are significant, as in EV charging scenarios. To tackle this problem, several solutions are proposed in the literature, which can be grouped into four categories. The first one is to add additional stages in order to reduce the gain requirements of the CLLC converter, either before the resonant converter, as presented in [15], where the previous Power Factor Correction (PFC) stage of the converter is modified in order to achieve a variable DC-link voltage, or after it, like in [16], where an additional buck converter is added after the resonant converter, making the gain of the resonant tank unitary for the whole working range.

A second option is implementing reconfigurable circuits in the primary and/or secondary side of the transformer. A hybrid half-bridge/full-bridge inverter is proposed in [17], allowing the system to double the resonant tank input voltage. In [18] a hybrid rectifier in the secondary side is presented, which allows the system to go from a full diode bridge to an asymmetrical half bridge that acts as a voltage doubler.

Control and modulation strategies are other options to improve the voltage gain performance of the system. A frequency control with an adjustable duty cycle is presented in [19], which improves the light load efficiency of the converter. In [20], a hybrid control strategy that combines Pulse Frequency Modulation (PFM) with Phase Shift Modulation (PSM) is presented, which improves the efficiency of the system over the whole operating range compared to its non-hybrid counterparts.

Finally, adjustable resonant tanks can also be found in the literature. A reconfigurable transformer is presented in [21], allowing a variable turn ratio that increases the gain of the tank. Different variable resonant components are presented in [22]–[25], where the value of the resonant inductance, the magnetizing inductance, or both can be controlled to change the characteristics of the gain curve according to the needs of the system.

Converters with reconfigurable resonant tanks are another option to improve the system's gain response. In [26], a commutable additional capacitor in parallel with the resonant inductor of the primary side is added, making the system work as a CLLC converter in boost operation and as a C-CL-LC in reduction operation. A commutable inductor in parallel with the primary side of the resonant tank is presented in [27], which improves the boost operation in reverse mode.

This paper focuses on solving the main challenges presented until now, which consist of reaching the gain requirements of the system while:

- Operating at a valid frequency range.
- Switching with ZVS all over the working range.

- Not compromising the main power direction design in a bidirectional converter.

To achieve this, paving the way to unifying the voltage regulation of the converter into a single step, this paper focuses on the DC/DC stage of a bidirectional battery charger. For this, a converter as shown in Fig. 1 has been designed, which consists of two full bridge synchronous inverters/rectifiers, depending on the power flow direction, and a reconfigurable resonant tank that can be alternated between CLLC, i.e. C3LC, and CLLLC, i.e. C4LC, by adding an additional inductance in parallel with the resonant components of the primary side, and studies its effects. This additional component further improves the gain characteristics and switching frequency range for reverse operation mode, allowing an optimal design of the tank in forward mode, all while ensuring ZVS in every scenario.

The study aims to provide a comprehensive understanding of the benefits and trade-offs involved in adding a commutable inductance in the resonant tank, supported by theoretical analysis and simulation results. The impact of the resonant tank asymmetries on the behavior of the tank is studied based on First Harmonic Approximation (FHA). With these results, a clear design process for asymmetrical resonant tanks is presented, including the selection of the additional component value.

In section II, the working principles of a conventional C3LC converter and the proposed C4LC are studied for both symmetrical and asymmetrical tanks to identify the problematic of working bidirectionally with the same resonant tank configuration. The proposed solution is then compared to the conventional approach to see how it affects the response of the system. To further prove the validity of this proposal, a C4LC converter is designed for a real application scenario in section III, where both the C4LC and C3LC configuration performances are compared by simulation. Finally, the conclusions are presented in section IV.

II. Analysis of a C4LC converter

The previously presented converter shown in Fig. 1 consists of a reconfigurable resonant tank connected to the input and output by full-bridge switching networks both on the primary and secondary sides. The resonant tank configuration can be switched between C3LC and C4LC topologies using the switch S_p, which adds an additional L_p inductance in parallel between the resonant components L_{r_1} and C_{r_1} in the primary side.

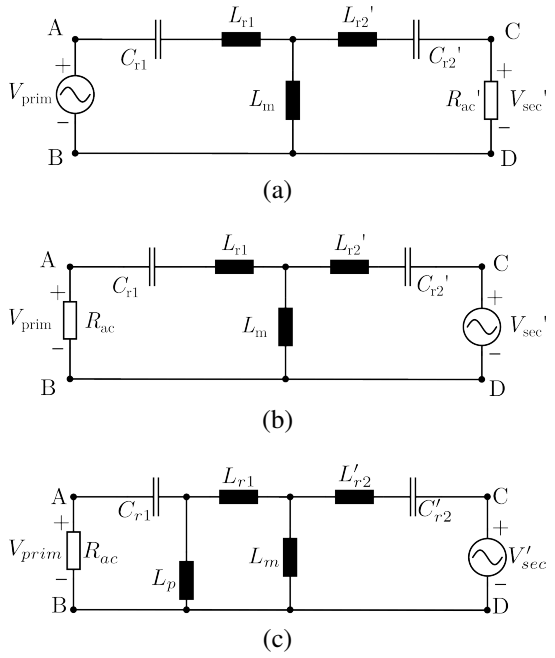

Fig. 2. FHA model of the resonant tank in Fig. 1 with all components referred to the primary side in (a) forward mode and (b) reverse mode for the C3LC topology and (c) reverse mode for the C4LC topology.

TABLE I
Main relations of the FHA

Parameter	Meaning
$R_{ac} = 8/\pi^2 R_{L,DC}$	Equivalent AC resistance of the load
$R'_{ac} = n^2 R_{ac}$	R_L referenced to the primary side
$L'_{r2} = n^2 L_{r2}$	L_{r2} referenced to the primary side
$C'_{r2} = C_{r2}/n^2$	C_{r2} referenced to the primary side
$f_{r,f} = 1/(2\pi\sqrt{L_{r1}C_{r1}})$	Forward resonant frequency
$f_{r,r} = 1/(2\pi\sqrt{L'_{r2}C'_{r2}})$	Reverse resonant frequency
$f_{r,p} = 1/(2\pi\sqrt{L_{rp}C_{r1}})$	Reverse parallel resonant frequency
$a = n^2 L_{r2}/L_{r1}$	Resonant inductor ratio
$b = C_{r2}/(n^2 C_{r1})$	Resonant capacitor ratio
$h_f = L_m/L_{r1}$	Forward tank inductor ratio
$h_r = L_m/(L'_{r2})$	Reverse tank inductor ratio
$h_p = L_m/L_p$	Parallel tank inductor ratio
$f_{n,f} = f_{sw}/f_{r,f}$	Forward normalized switching frequency
$f_{n,r} = f_{sw}/f_{r,r}$	Reverse normalized switching frequency
$Q_f = \sqrt{L_{r1}/C_{r1}}/R'_{ac}$	Forward quality factor
$Q_r = \sqrt{L'_{r2}/C'_{r2}}/R_{ac}$	Reverse quality factor

A. FHA analysis

The analysis begins with the fundamental principles of C3LC resonant converters, as shown in Fig. 1, highlighting the role of switching frequency, resonant tank components, and load variations in defining the

$$G_{\mathrm{f}} = \left| \frac{1/n}{\left(1 - \frac{1-f_{\mathrm{n,f}}^2}{h_{\mathrm{f}} \cdot f_{\mathrm{n,f}}^2}\right) - i\left(\frac{Q_{\mathrm{f}}}{f_{\mathrm{n,f}}}\left(\frac{1-ab \cdot f_{\mathrm{n,f}}^2}{b}\right)\left(1 - \frac{1-f_{\mathrm{n,f}}^2}{h_{\mathrm{f}} \cdot f_{\mathrm{n,f}}^2}\right) + \frac{Q_{\mathrm{f}}}{f_{\mathrm{n,f}}}\left(1 - f_{\mathrm{n,f}}^2\right)\right)} \right| \tag{1}$$

$$G_{\mathrm{r}} = \left| \frac{n}{\left(1 - \frac{1-ab \cdot f_{\mathrm{n,r}}^2}{b \cdot h_{\mathrm{r}} \cdot f_{\mathrm{n,r}}^2}\right) - i\left(\frac{Q_{\mathrm{r}}}{f_{\mathrm{n,r}}}\left(1 - f_{\mathrm{n,r}}^2\right)\left(1 - \frac{1-ab \cdot f_{\mathrm{n,r}}^2}{b \cdot h_{\mathrm{r}} \cdot f_{\mathrm{n,r}}^2}\right) + \frac{Q_{\mathrm{r}}}{f_{\mathrm{n,r}}}\left(\frac{1-ab \cdot f_{\mathrm{n,r}}^2}{b}\right)\right)} \right| \tag{2}$$

$$G_{\mathrm{r,p}} = \left| \frac{n \cdot i\frac{f_{\mathrm{n,r}}}{Q_{\mathrm{r}}}}{\left(1 - f_{\mathrm{n,r}}^2\right)\left(1 - \frac{h_{\mathrm{p}}}{h_{\mathrm{r}} \cdot f_{\mathrm{n,r}}^2}\right)\left(i\frac{f_{\mathrm{n,r}}}{Q_{\mathrm{r}}} + b\right) + \left(1 - \frac{1-f_{\mathrm{n,r}}^2}{h_{\mathrm{r}} \cdot f_{\mathrm{n,r}}^2}\right)\left(i\frac{f_{\mathrm{n,r}}}{Q_{\mathrm{r}}} + b - \frac{f_{\mathrm{n,r}}^2}{a} + \frac{h_{\mathrm{p}}}{a \cdot h_{\mathrm{r}}}\left(i\frac{f_{\mathrm{n,r}}}{Q_{\mathrm{r}}} + b\right)\right)} \right| \tag{3}$$

$$Z_{\mathrm{in,f}} = R'_{\mathrm{ac}} \frac{\left(1 - f_{\mathrm{n,f}}^2\right)\left(1 - ab \cdot f_{\mathrm{n,f}}^2 + i \cdot b\frac{f_{\mathrm{n,f}}}{Q_{\mathrm{f}}} - b \cdot h_{\mathrm{f}} \cdot f_{\mathrm{n,f}}^2\right) - h_{\mathrm{f}} \cdot f_{\mathrm{n,f}}^2\left(1 - ab \cdot f_{\mathrm{n,f}}^2 + i \cdot b\frac{f_{\mathrm{n,f}}}{Q_{\mathrm{f}}}\right)}{i\frac{f_{\mathrm{n,f}}}{Q_{\mathrm{f}}}\left(i \cdot b\frac{f_{\mathrm{n,f}}}{Q_{\mathrm{f}}} - f_{\mathrm{n,f}}^2\left(ab + b \cdot h_{\mathrm{f}}\right) + 1\right)} \tag{4}$$

$$Z_{\mathrm{in,r}} = R_{\mathrm{ac}} \frac{\left(1 - f_{\mathrm{n,r}}^2\right)\left(1 - \frac{f_{\mathrm{n,r}}^2}{ab} + i\frac{f_{\mathrm{n,r}}}{Q_{\mathrm{r}}}/b - h_{\mathrm{r}}/b \cdot f_{\mathrm{n,r}}^2\right) - h_{\mathrm{r}} \cdot f_{\mathrm{n,r}}^2\left(1 - f_{\mathrm{n,r}}^2/ab + i\frac{f_{\mathrm{n,r}}}{Q_{\mathrm{r}}}/b\right)}{i\frac{f_{\mathrm{n,r}}}{Q_{\mathrm{r}}}\left(i\frac{f_{\mathrm{n,r}}}{Q_{\mathrm{r}}}/b - f_{\mathrm{n,r}}^2\left(1 + a \cdot h_{\mathrm{r}}\right)/ab + 1\right)} \tag{5}$$

$$Z_{\mathrm{in,r,p}} = \frac{R_{\mathrm{ac}}}{i\frac{f_{\mathrm{n,r}}}{Q_{\mathrm{r}}}}\left(\left(1 - f_{\mathrm{n,r}}^2\right) - \frac{f_{\mathrm{n,r}}^2\left(\left(1 + i\frac{f_{\mathrm{n,r}}}{b \cdot Q_{\mathrm{r}}} - f_{\mathrm{n,r}}^2\frac{h_{\mathrm{r}}}{b \cdot h_{\mathrm{p}}}\right)/a + \frac{h_{\mathrm{r}}}{h_{\mathrm{p}}}\left(1 + i\frac{f_{\mathrm{n,r}}}{b \cdot Q_{\mathrm{r}}}\right)\right)}{\left(1 + \frac{1}{h_{\mathrm{r}}}\right)\left(1 + i\frac{f_{\mathrm{n,r}}}{b \cdot Q_{\mathrm{r}}} - f_{\mathrm{n,r}}^2\frac{h_{\mathrm{r}}}{b \cdot h_{\mathrm{p}}}\right) + \frac{1}{h_{\mathrm{p}}}\left(1 + i\frac{f_{\mathrm{n,r}}}{b \cdot Q_{\mathrm{r}}}\right)}\right) \tag{6}$$

converter's operation. FHA is used to analyze the tank's response. With this approximation and referring the secondary side components to the primary side, the resonant tank can be simplified, as shown in Fig 2.

Applying Kirchhoff's Current Law (KCL) and Kirchhoff's Voltage Law (KVL) in the circuits of Fig. 2 and considering the relations presented in Table I, the voltage gain equation of the resonant tank can be deduced for forward mode (1), reverse C3LC mode (2) and reverse C4LC mode (3). Similarly, the input impedance of the resonant tank is defined as (4) for forward mode, (5) for reverse C3LC mode, and (6) for reverse C4LC mode.

It can be seen how all the gain equations (1)-(3) and the phase of the input impedance equations (4)-(6) are only dependent on five parameters, all defined in Table I: the quality factor and tank inductor ratio in forward mode, Q_{f} and h_{f}, and their equivalent forms in reverse mode Q_{r} and h_{r}, which define the values of the primary side components as well as the response of the system under different load conditions. Additionally, the transformer turn ratio, n, the resonant inductor ratio, a, and the resonant capacitor ratio, b determine the level of asymmetry between the primary and the secondary side, and define the behavior of the system in reverse mode. Therefore, it is crucial to analyze the effect each of these parameters has on the performance of the system. Therefore, it is crucial to analyze the effect each of these parameters has on the performance of the system.

B. Analysis of a symmetrical tank

When the resonant tank is symmetrical, meaning that all component values are identical ($a = 1$, $b = 1$) and the transformer turn ratio is $n = 1$, the gain relations, as well as the input impedances are the same for forward and reverse mode, meaning that the gain of the resonant tank is the same both in forward and in reverse mode, $G_{\mathrm{f}} = G_{\mathrm{r}}$, and that the same thing happens

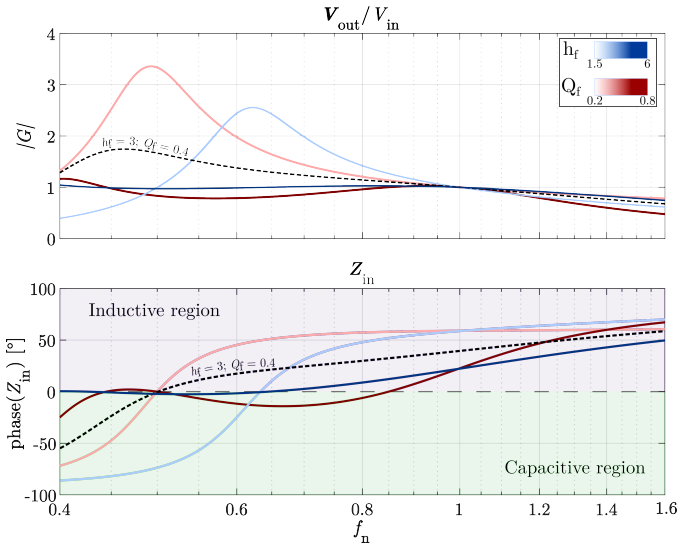

Fig. 3. Voltage gain and input impedance phase for different $h_f = h_r$ values (a) and $Q_f = Q_r$ values (b) when the resonant tank is symmetrical. The dashed line represents the response of a given h_f - Q_f combination, and the blue colored lines represent variations of h_f for a constant Q_f while the red lines represent variations of Q_f for a constant h_f, affecting both the gain $|G|$ and the impedance Z_{in} of the resonant tank.

with the impedance of the tank, $Z_{in,f} = Z_{in,r}$. Both these expressions are represented in Fig. 3.

In Fig. 3, it can be seen how, for a fixed Q_f value, changing the value of h_f alters the behavior of the system. First, the maximum achievable gain increases as h_f decreases. Additionally, as the value of h_f increases, the capacitive/inductive boundary shifts to the left, causing the peak of the gain curve to occur at a lower normalized switching frequency. Consequently, a value further from the resonant frequency is needed to achieve the maximum voltage gain. Nevertheless, for a h_f higher than a critical value, the curve becomes non-monotonic, making the behavior of the system more complex. Finally, lower h_f values would imply greater circulating currents, increasing the overall power losses. Additionally, analyzing the Z_{in} phase graph, a critical factor can be appreciated when the value of h_f is too high: the inductive behavior of the tank is lost in the operating frequency range (frequencies above the point where the Z_{in} phase crosses 0°), which is essential for the system to work with ZVS.

Something similar happens for a fixed h_f and variable Q_f when looking at Fig. 3: the maximum gain of the resonant tank increases when Q_f decreases, while the peak value of the gain curve shifts to the left, widening the bandwidth of the tank. In this case, the inductive behavior of the tank is also lost in the operating frequency range if Q_f is above a critical value.

Therefore, the design of the resonant tank components must consider not only the maximum and minimum gains required by the specifications but also the critical h_f and Q_f values to stay within the inductive region through the whole operating frequency range, all why maintaining the monotonicity of the gain curve. Additionally, since a reduced operating frequency range is convenient, the effect of h_f and Q_f in this factor should also be considered.

C. Analysis of an asymmetrical tank

When the design of the tank is asymmetrical, meaning that either $a \neq 1$, $b \neq 1$, or $n \neq 1$, the tank behavior in reverse mode changes notably compared to the forward mode. All these three scenarios have been analyzed for a constant working point and are represented in Fig. 4.

Analyzing the three asymmetries presented in 4, it can be seen how changing either a, b, or n changes the response of the system but affects the gain characteristics in reverse mode in a greater way than in forward mode. Consequently, an asymmetric tank will not only make the design of the converter more challenging, but it will also affect the performance of the tank in forward mode, something that should be avoided.

D. Adaptative resonant tank

The proposed solution consists of an adaptative resonant tank that works and is optimally designed to maximize the value of h_f as a regular C3LC converter in forward mode but that reconfigures into a C4LC when working in reverse operation mode. The resultant response of this topology is depicted in Fig. 5, where the response of the system is represented with a fixed C3LC configuration and adding different L_p values. Three main advantages can be seen: First, the maximum and minimum gains are extended, so the system is capable of meeting the requirements in a scenario where the C3LC may fail to do so. Additionally, the bandwidth of the tank is also narrowed, as both the peak gain and the minimum gain move towards the resonant frequency as the value of h_p increases.

Moreover, as mentioned before, the design of the forward operation mode is not constrained by the requirements of the reverse mode if this topology morphing strategy is applied, so it can be optimally designed without affecting its performance.

III. Design of a C4LC converter

After analyzing the response of both the C3LC and C4LC topologies, a bidirectional converter is designed

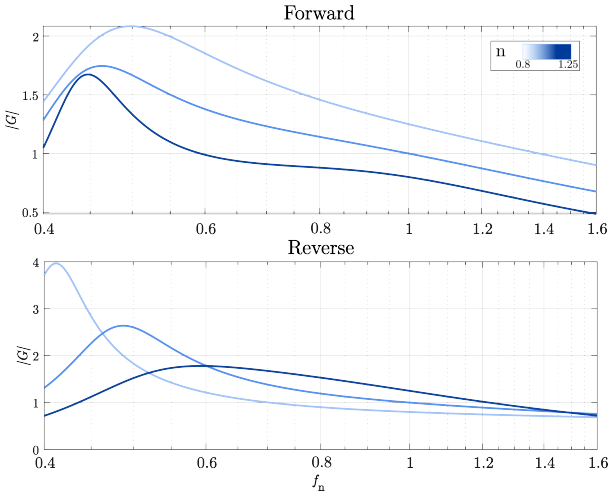

(a)

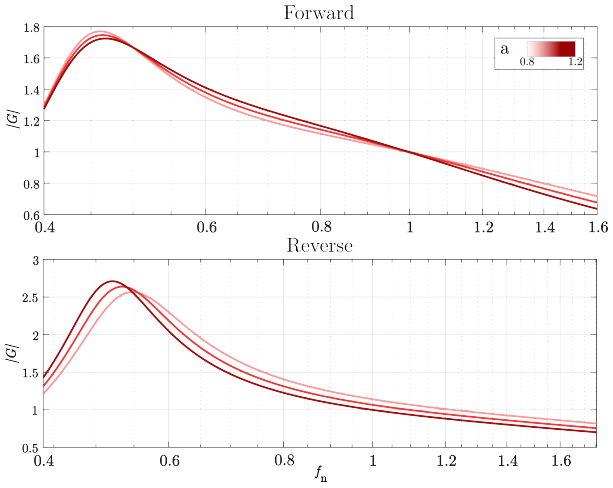

(b)

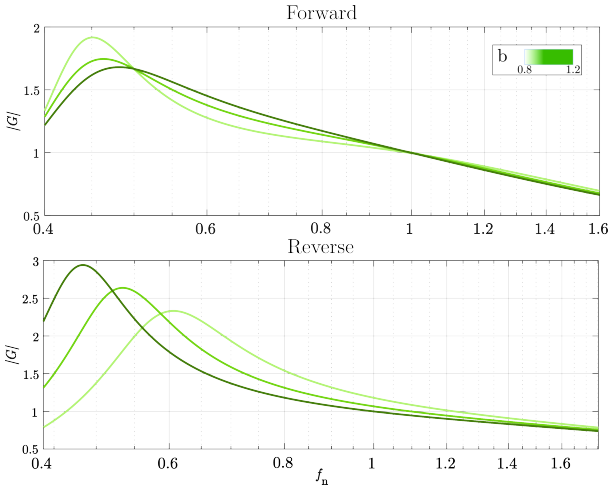

(c)

Fig. 4. Voltage gain in forward and reverse modes for different asymmetries: variable n in (a), variable $a = n^2 L_{r2}/L_{r1}$ in (b) and variable $b = C_{r2}/(n^2 C_{r1})$ in (c). The gain response of each scenario is represented both in forward and reverse mode for different variations of each asymmetry.

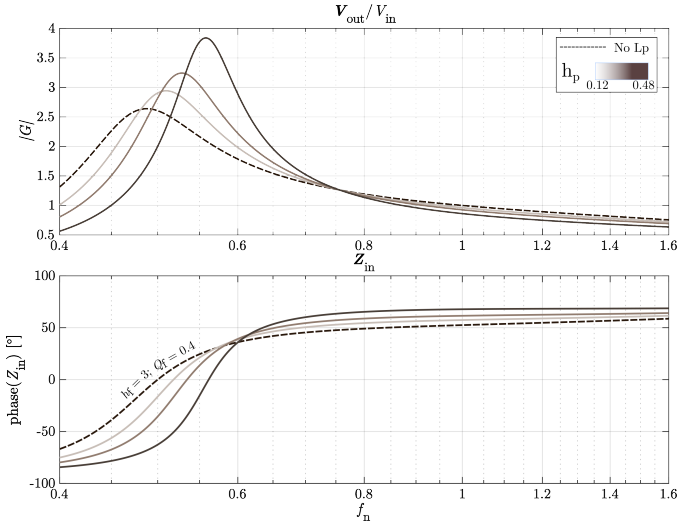

Fig. 5. Voltage gain and Z_{in} phase for different h_p values in reverse mode for a fixed C3LC configuration. The original response in Fig. 3 (No L_p in this figure) is compared to the response of the system adding an extra inductor in parallel in the primary side with an increasing value.

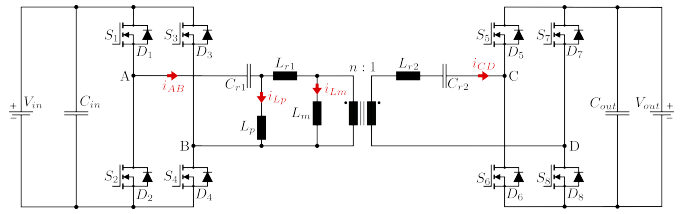

Fig. 6. C4LC resonant converter with the extra inductor L_p and the main signals of the resonant tank marked in red.

to validate the proposed topology in a real application scenario, as the one depicted in Fig. 6.

A. Case study

The specifications considered for the design process are displayed in Table II. From this data, the first step is to calculate the transformer turn ratio, obtained assuming unity gain for the resonant tank and nominal conditions:

$$n = V_{\text{in,nom}}/V_{\text{out}_n\text{om}} \tag{7}$$

From (7), the value of n can be calculated. Although a symmetric tank is the objective, in order to maintain optimum performance in forward mode, a non-unitary value of n causes a mismatch between the leakage inductances of the transformer. Since a higher power density is required, the leakage inductances of the transformer act as the resonant inductances L_{r1} and L_{r2}, and therefore, a non-unity value of a is obtained. Meanwhile, the value for the resonant capacitors C_{r1} and C_{r2} have been selected

TABLE II
DESIGN SPECIFICATIONS OF A BIDIRECTIONAL LITHIUM-ION BATTERY CHARGING SYSTEM USING GAN TRANSISTORS

Parameter	Charge value (nominal)	Discharge value (nominal)
V_{in} (V)	400 (400)	
V_{out} (V)	300 - 420 (320)	280 - 420 (320)
P (kW)	420 - 6.6 (5)	1 - 6.6 (3)
f_{sw} (kHz)	200 - 800 (500)	

to be equal, meaning that the resonant capacitor ratio is only dependent on the value of n. All the asymmetry factor values for this specific design are displayed in Table III.

With the mentioned transformer characteristics, considering the gain requirements from Table II, and based on the relations from Table I and equations 1-6, a set of valid h_f, Q_f and Q_r combinations can be obtained, considering that each of these combinations can achieve the required forward or reverse required gains inside the specified switching frequency range, maintaining an inductive behavior, and only considering valid curves that are monotonic inside the operating region. With these constraints, obtained results can be seen in Fig 7. The area below each of the curves in Fig. 7 covers all the valid h_f - $Q_{f/r}$ combinations for each of the operation modes. Since h_f is a fixed value of the resonant tank that is shared by both the forward and reverse modes, the design of the most restrictive operation mode affects the performance of the less restrictive one. However, the first step to choosing a value for h_f is delimiting the Q_f and Q_r operating ranges.

Considering that the parameters involving resonant tank values that appear in the Q_f and Q_r relations of Table I have a fixed value, and from the critical values for each R_L obtained from the specifications in Table II, it can be assumed that the following relation is true:

$$\frac{Q_{f,max}}{Q_{f,min}} = \frac{R_{L,out-max}}{R_{L,out-min}}; \frac{Q_{r,max}}{Q_{r,min}} = \frac{R_{L,in-max}}{R_{L,in-min}} \quad (8)$$

In order to define the inductance relation h_f of the resonant tank, a value around 10 or higher is desirable for integrated transformers [24], [25]. The Q_f and Q_r range widths are fixed, defined by the expressions in (8). Selecting an optimum h_f value ($h_{f,opt}$) for the fixed Q_f width, an operating range that exactly fits the requirements can be obtained, as well as specific values for $Q_{f,max}$ and $Q_{f,min}$.

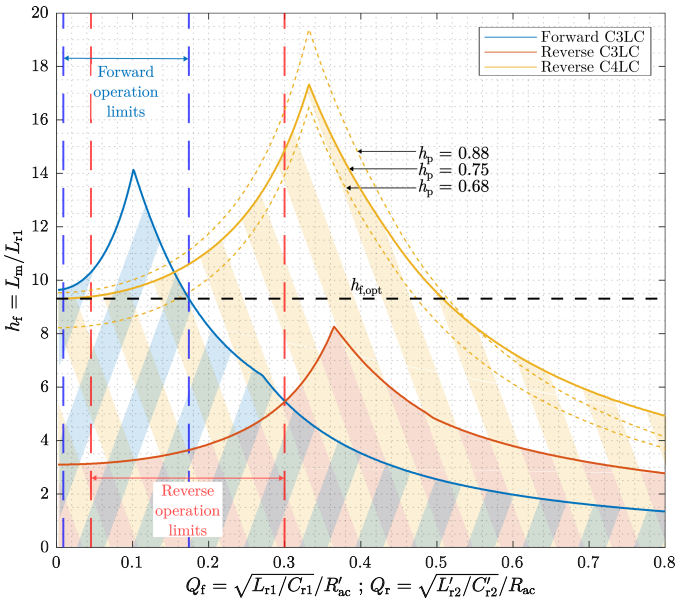

Fig. 7. Valid configurations of the different operating modes for the given specifications, defined by the colored curves and the whole marked area beneath them. h_f is selected so that the valid configuration curve in forward mode perfectly fits the forward operating range. This also determines the forward and reverse operating limits by fixing the Q_f and Q_r critical values. With h_f defined, h_p is selected so that the valid configuration curve in reverse mode for the C4LC resonant tank fits the reverse operating range limits while maintaining an h_p value as high as possible.

This can be better seen in Fig. 7 where, for the specified Q_f range, the operating region marked by the h_f line fits in the valid h_f-Q_f area inside the forward operating limits. Nevertheless, this is not true for the reverse C3LC operation, failing to meet the requirements all over the Q_r working region for $h_{f,opt}$.

B. Design considerations of additional parallel inductor

Considering the optimized design from the previous section, a C4LC configuration can be designed to fulfill the conditions in reverse mode. By choosing the proper h_p value, it can be seen in Fig. 7 how the operating region marked by the h_f line fits in the valid h_f-Q_r area of the C4LC topology inside the reverse operating limits, all without compromising the performance of the conventional C3LC in forward mode. With all the conditions just presented, the values of the resonant tank components can be calculated by selecting any point in the $h_{f,opt}$ line and considering the resonant frequency from II. They are all summarized in Table III.

Considering these values, the response of the system for the operation limits is marked in Fig. 7, and is represented in Fig. 8. It can be seen how, for the C3LC topology, the gain requirements are not fulfilled in

TABLE III
DESIGNED PARAMETERS

Parameter	Value	Relation
n	1.25	-
$L_1(\mu H)$	1.35	a = 1.25
$L_2(\mu H)$	1.07	
C_1(nC)	7.54	b = 0.64
C_2(nC)	7.54	
$L_m(\mu H)$	12.51	h_f = 9.34
$L_p(\mu H)$	16.76	h_p = 0.75

reverse mode for an optimum design in forward mode of $h_{f,opt}$, while reconfiguring the tank to a C4LC with the configuration presented in Table III in reverse mode solves this issue.

C. Discussion

Even if the solution presented in section III-A allows for an optimum design of the system for a maximized h_f value in forward mode while still fulfilling the requirements in reverse mode, it is true that the obtained value is slightly lower than the set minimum range limit set in section III-A. However, checking Fig. 7, a higher h_f value for the given specifications is not attainable.

With this configuration, the output voltage range in reverse mode without the additional inductor does not reach the minimum required gain, resulting in a battery voltage range 45 % smaller than required. However, with the proposed configuration, the additional component can be adjusted so that the acquirable voltage range remains at 100 % with a maximized h_f value for the forward mode. Furthermore, again using Fig. 7, it can be deduced that it is possible to reach the required gains for both power directions without adding L_p by reducing h_f to a low enough value. By redesigning the resonant tank, a C3LC configuration as presented in Table IV is obtained. Bigger values of Q_f and a lower value of h_f imply sharper gain curves, as deduced from Fig. 3, and this is translated in narrower frequency bandwidths. Specifically, the forward operating frequency range is reduced by 50 %, while the reverse range is reduced by 12.7 %.

However, the h_f relation decreases by 65 %, reaching a value of 3.25, far below the design criteria set in section III-A, which would result in a lower-performance transformer. Furthermore, a very small value, such as the one needed by the C3LC topology, makes it extremely challenging to design an integrated transformer that

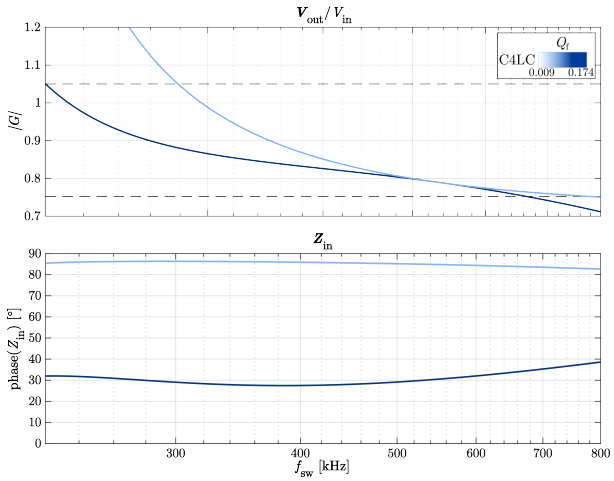

(a)

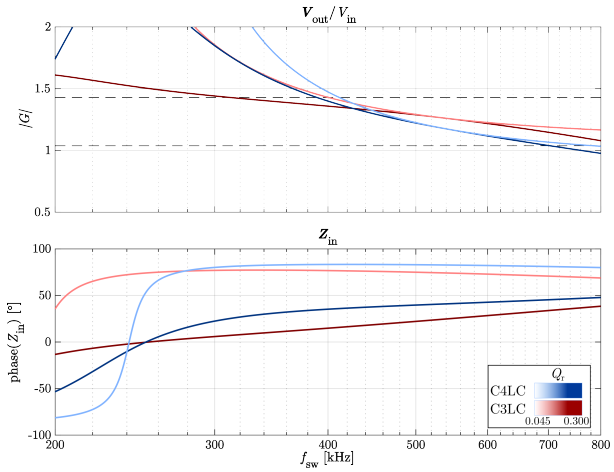

(b)

Fig. 8. Response of the system for the operation limits marked in Fig. 7 for (a) forward mode and (b) reverse mode.

fulfills the required characteristics, meaning that two additional external inductors will be required in the resonant tank. Nevertheless, the actual impact of this compared to the extra parallel inductor of the proposed topology is uncertain and requires further analysis.

IV. CONCLUSION

This paper explores the potential to improve the performance of CLLC converters for asymmetrical bidirectional operation by introducing an additional parallel inductor into the resonant tank, forming a C4LC configuration in reverse mode without affecting the forward operation. Theoretical analysis and simulations demonstrate improvements in gain characteristics for the reverse mode operation without affecting the forward mode performance.

TABLE IV
TOPOLOGY COMPARISON

Parameter	C3LC	C4LC
L_r (μH)	3.06	1.34
C_r (nC)	3.31	7.54
L_m (μH)	9.94	12.51
L_p (μH)	-	16.76
h_r	3.25	9.34
Forward		
f_{sw} (kHz)	264 - 562	200 - 800
Reverse		
f_{sw} (kHz)	442 - 800	390 - 800

Comparing the C4LC topology with an optimum conventional C3LC design, even though the proposal impacts the switching frequency range, the proposed converter is capable of increasing the reverse mode voltage gain range by 1.82 without compromising the forward operation optimum design for a maximized h_f, meeting the design requirements. In this note, an h_f parameter 2.87 times bigger has been achieved compared to an optimum C3LC design, obtaining a final value of 9.34 and making it viable to integrate the resonant inductors in the transformer without compromising its performance. However, it is unclear how beneficial this will turn out to be for the overall size of the system, considering that the proposal includes an extra inductor to the tank. In addition, the switching frequency range is significantly increased for the proposed system, a key factor that may have a negative effect on its performance.

REFERENCES

[1] J. Yuan, L. Dorn-Gomba, A. D. Callegaro, J. Reimers, and A. Emadi, "A Review of Bidirectional On-Board Chargers for Electric Vehicles," *IEEE Access*, vol. 9, pp. 51501–51518, 2021.

[2] S. Islam, A. Iqbal, M. Marzband, I. Khan, and A. M. A. B. Al-Wahedi, "State-of-the-art vehicle-to-everything mode of operation of electric vehicles and its future perspectives," *Renewable and Sustainable Energy Reviews*, vol. 166, p. 112574, Sept. 2022.

[3] M. Yilmaz and P. T. Krein, "Review of the Impact of Vehicle-to-Grid Technologies on Distribution Systems and Utility Interfaces," *IEEE Transactions on Power Electronics*, vol. 28, pp. 5673–5689, Dec. 2013.

[4] S. Deshmukh (Gore), A. Iqbal, S. Islam, I. Khan, M. Marzband, S. Rahman, and A. M. A. B. Al-Wahedi, "Review on classification of resonant converters for electric vehicle application," *Energy Reports*, vol. 8, pp. 1091–1113, Nov. 2022.

[5] G. A. Mudiyanselage, N. Keshmiri, and A. Emadi, "A Review of DC-DC Resonant Converter Topologies and Control Techniques for Electric Vehicle Applications," *IEEE Open Journal of Power Electronics*, vol. 4, pp. 945–964, 2023.

[6] C. Schell, "Here's why we need a smart grid — and how we build one." https://www.weforum.org/agenda/2022/12/the-future-of-smart-energy-is-systemic-open-and-collaborative/, Dec. 2022.

[7] M. Rezayati, F. Tahami, J.-L. Schanen, and B. Sarrazin, "Generalized State-Plane Analysis of Bidirectional CLLC Resonant Converter," *IEEE Transactions on Power Electronics*, vol. 37, pp. 5773–5785, May 2022.

[8] J.-H. Jung, H.-S. Kim, M.-H. Ryu, and J.-W. Baek, "Design Methodology of Bidirectional CLLC Resonant Converter for High-Frequency Isolation of DC Distribution Systems," *IEEE Transactions on Power Electronics*, vol. 28, pp. 1741–1755, Apr. 2013.

[9] K. Siebke and R. Mallwitz, "Comparison of a Dual Active Bridge and CLLC Converter for On-Board Vehicle Chargers using GaN and Time Domain Modeling Method," in *2020 IEEE Energy Conversion Congress and Exposition (ECCE)*, pp. 1210–1216, Oct. 2020.

[10] B. McDonald, "CLLLC vs. DAB for EV onboard chargers," tech. rep., Texas Instruments, Dallas, Texas, 2021.

[11] P. He and A. Khaligh, "Comprehensive Analyses and Comparison of 1 kW Isolated DC–DC Converters for Bidirectional EV Charging Systems," *IEEE Transactions on Transportation Electrification*, vol. 3, pp. 147–156, Mar. 2017.

[12] M. Kim, H. Jeong, B. Han, and S. Choi, "New Parallel Loaded Resonant Converter With Wide Output Voltage Range," *IEEE Transactions on Power Electronics*, vol. 33, pp. 3106–3114, Apr. 2018.

[13] M. Bhardwaj and S.-Y. Yu, "Bidirectional CLLLC Resonant Dual Active Bridge (DAB) Reference Design forHEV/EV Onboard Charger," tech. rep., Texas Instruments, Dallas, Texas, 2019.

[14] M. Bartecka, M. Kłos, and J. Paska, "Effective Design Methodology of CLLC Resonant Converter Based on the Minimal Area Product of High-Frequency Transformer," *Energies*, vol. 17, p. 55, Jan. 2024.

[15] B. Li, F. C. Lee, Q. Li, and Z. Liu, "Bi-Directional On-Board Charger Architecture and Control for Achieving Ultra-High Efficiency with Wide Battery Voltage Range," in *2017 IEEE Applied Power Electronics Conference and Exposition (APEC)*, pp. 3688–3694, Mar. 2017.

[16] F. Jin, A. Nabih, C. Chen, X. Chen, Q. Li, and F. C. Lee, "A High Efficiency High Density DC/DC Converter for Battery Charger Applications," in *2021 IEEE Applied Power Electronics Conference and Exposition (APEC)*, (Phoenix, AZ, USA), pp. 1767–1774, IEEE, June 2021.

[17] L. A. D. Ta, N. D. Dao, and D.-C. Lee, "High-Efficiency Hybrid LLC Resonant Converter for On-Board Chargers of Plug-In Electric Vehicles," *IEEE Transactions on Power Electronics*, vol. 35, pp. 8324–8334, Aug. 2020.

[18] Y. Shen, H. Wang, A. Al-Durra, Z. Qin, and F. Blaabjerg, "A Structure-Reconfigurable Series Resonant DC–DC Converter With Wide-Input and Configurable-Output Voltages," *IEEE Transactions on Industry Applications*, vol. 55, pp. 1752–1764, Mar. 2019.

[19] S.-H. Ryu, D.-H. Kim, M.-J. Kim, J.-S. Kim, and B.-K. Lee, "Adjustable Frequency–Duty-Cycle Hybrid Control Strategy for Full-Bridge Series Resonant Converters in Electric Vehicle Chargers," *IEEE Transactions on Industrial Electronics*, vol. 61, pp. 5354–5362, Oct. 2014.

[20] L. Mulder, *Hybrid Control Strategy for Bi-Directional CLLC DC-DC Converters in Electric Vehicle Onboard Chargers*. PhD thesis, Eindhoven University of Technology, Eindhoven, Oct. 2022.

[21] H. Wang, M. Shang, and D. Shu, "Design Considerations of Efficiency Enhanced LLC PEV Charger Using Reconfigurable Transformer," *IEEE Transactions on Vehicular Technology*, vol. 68, pp. 8642–8651, Sept. 2019.

[22] Y. Wei and A. Mantooth, "A family of LLC converters with magnetic control," in *Conference Proceedings - IEEE Applied Power Electronics Conference and Exposition - APEC*, pp. 783–789, 2021.

[23] V. Costa, M. Perdigão, A. Mendes, and J. Alonso, "Evaluation of a variable-inductor-controlled LLC resonant converter for battery charging applications," in *IECON Proceedings (Industrial Electronics Conference)*, pp. 5633–5638, 2016.

[24] D.-K. Kim, C.-O. Yeon, J.-H. Kim, Y. Jeong, and G.-W. Moon, "LLC resonant converter with high voltage gain using auxiliary LC resonant circuit," in *9th International Conference on Power Electronics - ECCE Asia: "Green World with Power Electronics", ICPE 2015-ECCE Asia*, pp. 1505–1512, 2015.

[25] J.-H. Teng, S.-S. Chen, Z.-X. Chou, and B.-H. Liu, "Novel Half-Bridge LLC Resonant Converter With Variable Resonant Inductor," *IEEE Transactions on Industry Applications*, vol. 59, no. 6, pp. 6952–6962, 2023.

[26] R. Reddy and M. Das, "Reconfigurable Resonant DC-DC Bidirectional Converter for Wide Output Voltage Applications," *IEEE Transactions on Industry Applications*, vol. 60, no. 1, pp. 573–583, 2024.

[27] X. Zhou, C. Chen, Z. Xu, K. Ni, T. Yang, and J. Zhang, "An Improved Bidirectional Variable Structure LLC Resonant Converter," in *2022 IEEE 3rd China International Youth Conference on Electrical Engineering, CIYCEE 2022*, 2022.